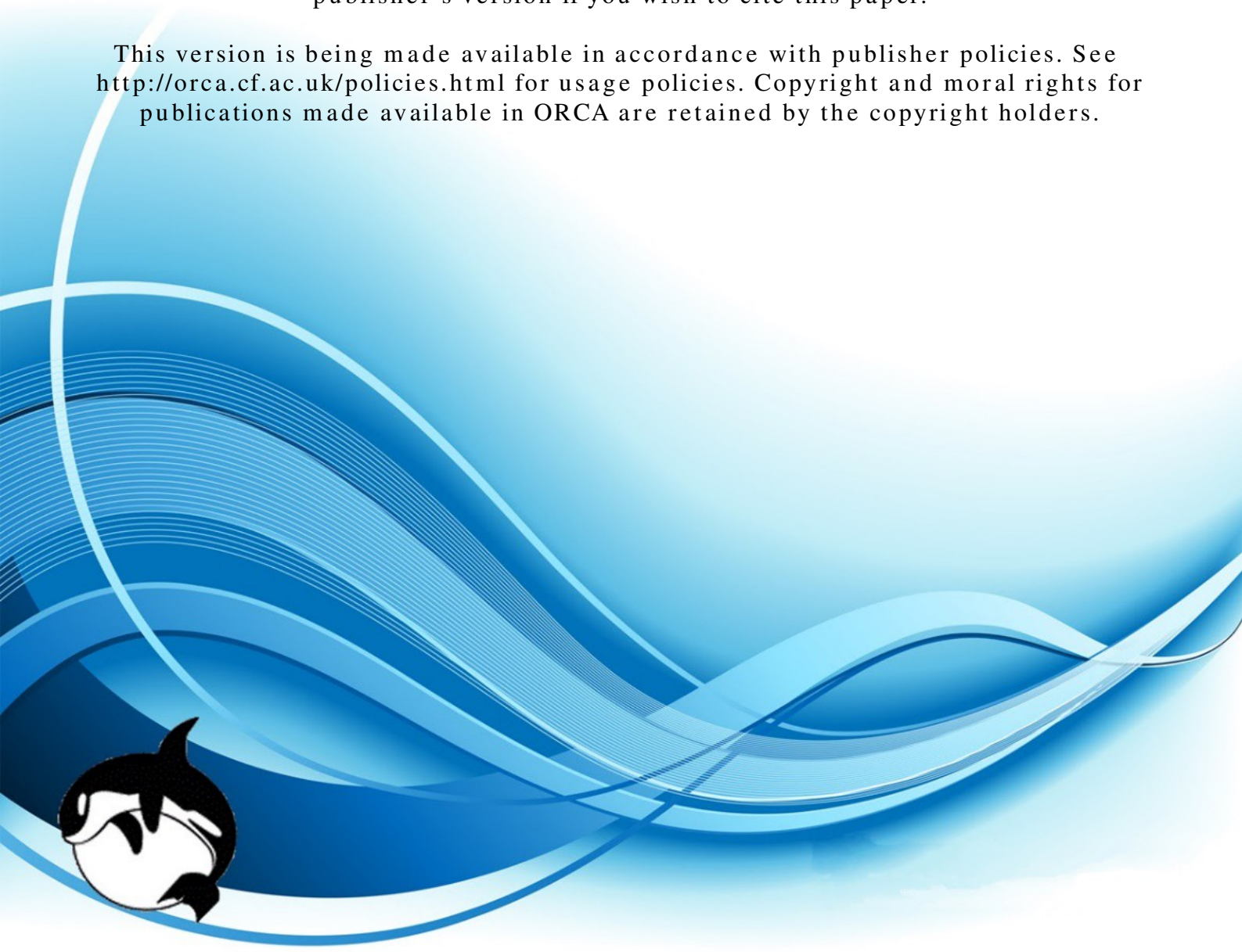

A Deep Learning Approach to Recover High-g Shock Signals from the Faulty Accelerometer

Jingjing Wen, Houpu Yao, *Student Member, IEEE*, Bin Wu, Yi Ren, and Ze Ji, *Member, IEEE*

***Abstract*—A deep learning based approach is proposed to accurately recover shock signals measured from a damaged high-g accelerometer without modifying the hardware. We first conducted shock tests and collected a large dataset of shock signals with different levels of acceleration by using an efficient experimental apparatus. The training data is composed of a pair of signals simultaneously obtained from a faulty accelerometer and a high-end accelerometer (served as the ground truth). A customized autoencoder neural network is designed and trained on this dataset, aiming to map the faulty signals to their reference counterparts. Experimental results show that, with the help of deep learning, shock signals can be accurately recovered from the faulty measurements. Compared with conventional approaches that require diagnosing and replacing faulty parts, the proposed data-driven method demonstrates a highly promising solution that allows recovering corrupted signals without introducing extra work to upgrade the hardware at almost zero cost. The dataset and code of this work are made publicly available on GitHub at https://github.com/hope-yao/Sensor_Calibration.**

***Index Terms*—Autoencoder, deep learning, data recovery, high-g accelerometer, shock test**

I. Introduction

Shock loading, especially the high-g level shock, is characterized as a transient transfer of massive energy to a system, which is very likely to seriously affect the performance of the system [1]. Many conditions, such as the release of space equipment [2], drop of electronic devices [3], and crashing of vehicles [4], are subjected to high-g shock excitations. In order to estimate and improve the reliability of products under shocks, high-g accelerometers are developed and widely used to measure shock responses [5]. However, accurately measuring a high-g shock signal is challenging because of the high peak value, short duration, and complicated frequency spectrum [6]. To obtain an accurate measurement, many efforts have been devoted to improving the hardware of sensors [7]. One of the drawbacks is the high hardware cost. Besides, diagnosing faulty accelerometers can be very time consuming. Moreover, due to the intellectual protections with different corporations, it is difficult to correct faulty accelerometers by upgrading the inner sensing units directly. Thus, it would be of great interest to sensor manufacturers as well as end-users to develop an efficient and low-cost method that can extend the lifecycle of accelerometers by recovering accurate results from corrupted signals measured with faulty accelerometers.

To improve the measuring performance of high-g accelerometers, sensor calibration is always required to characterize the systematic errors of individual sensors. Two main shock calibration methods are described by the International Organization for Standardization: the primary shock calibration method [8] and the comparative calibration method [9]. The former is accurate but expensive, whereas the latter is convenient but with slightly lower accuracy. An example of the primary shock calibration is the Hopkinson bar system [10], which is able to generate high-g shock loadings with an air gun and measure shock signals accurately via laser interferometry. The typical comparative calibration approach is termed as "back-to-back" method [11], which calibrates a sensor by comparing it with a calibrated reference transducer. These methods have been widely employed to calibrate the dynamic linearity, sensitivity, and repeatability of a raw accelerometer. Nevertheless, these methods can only test the precision of an accelerometer but lack the competence of improving its measuring performance.

Researchers have tried to improve the performance of sensors by mapping the raw electrical signals of an accelerometer to its calibrated counterparts. Such methods include looking-up table and nonlinear fitting [12], [13]. However, these methods suffer from poor generalization performance and low calibration accuracy. Besides, these methods entirely rely on the high repeatability of the accelerometer. Lastly, these mapping methods cannot calibrate the entire time-domain shock signal but merely the peak value and/or pulse width of a shock signal [14]. Only the two parameters (peak value and pulse width), though they are two key parameters in conventional standard-waveform-based shock test [1], cannot describe the actual shock environment exactly. The shock response spectrum (SRS) method, which converts the entire time-domain shock signal into a frequency-domain spectrum, is proposed for signal characterization and replacing the standard-waveform-based shock test methods gradually, especially in pyroshock test [2], [6]. Therefore, it is important to enhance the capability of recovering the entire time-domain shock signal from the faulty

Manuscript submitted July 30, 2019. This work was sponsored by Innovation Foundation for Doctor Dissertation of Northwestern Polytechnical University (No. CX201902).

J. Wen and B. Wu are with the School of Astronautics, Northwestern Polytechnical University, Xi'an 710072, China (email: wjj1990@mail.nwpu.edu.cn; wubin@nwpu.edu.cn). J. Wen is also the Research Associate in the School of Engineering, Cardiff University, Cardiff CF243AA, UK (email: wenj8@cardiff.ac.uk).

H. Yao and Y. Ren are with the Department of Mechanic and Aerospace Engineering, Arizona State University, Tempe 85281, USA (email: hope-yao@asu.edu; yren32@asu.edu)

Z. Ji is with the School of Engineering, Cardiff University, Cardiff CF243AA, UK (email: jiz1@cardiff.ac.uk).

Corresponding author: B. Wu and Z. Ji.

J. Wen and H. Yao contributed equally to this work.

shock signals instead of only the peak value and pulse width. Meanwhile, the peak value of a shock signal is a significant index in board-level shock tests after all [3]. Thus, it is critical that the proposed recovery method should be able to recover the holistic time-domain signal waveform while remain high calibration accuracy on the signals' peak values.

Over the past decade, deep learning has achieved great success in a variety of fields. Examples include computer vision [15], fault diagnosis in mechanics [16], aerospace engineering [17], etc. However, few works have been done to introduce deep learning to the field of calibrating industrial high-g accelerometer. A related work is implemented by Oh *et al*. [18], in which a robots-used multi-axial force/torque sensor is calibrated based on deep learning and several problems, such as nonlinearity, errors, and coupling, are solved successfully. Besides, self-validating techniques have been applied to recover faulty data in the fields of pressure sensors [19], gas detectors [20], and temperature sensors [21]. Nevertheless, differing from the force/torque sensors, pressure sensors, gas detectors, and temperature sensors working on a low-amplitude and quasi-static environment, high-g accelerometers work under severe shock environments, and, hence, present strong nonlinear characteristics in terms of high amplitude, transient excitation time, and complicated frequency components [6]. These strong nonlinearities also lead to strong uncertainty in the high-g shock signals and thus make the training of deep neural network (DNN) more difficult [22]. Additionally, training data in [18] is obtained via simplified models, whereas it is quite difficult to build such models for high-g shock conditions due to the strong nonlinearity and uncertainty [23]. On the other hand, the self-validating techniques depend on physical or analytical redundancy, which makes these techniques more suitable for correcting faulty measurement of sensor arrays, but not the standalone high-g accelerometers.

In this work, instead of ameliorating hardware, a purely data-driven approach is proposed to recover the shock signals measured from the faulty accelerometer with the help of deep learning. The rationale of our work is that the hidden mapping between the faulty and normal shock signals can be mined via training DNN, and then recovering the corrupted signals by using the acquired mapping. The aim is to approximate the recovered shock signals to their reference counterparts, so that the faulty accelerometer could acquire similar measuring results with the high-end one, and thus the high-cost hardware repairing and time-consuming repeated shock tests could be avoided. This recovery method could be a valuable option to address some intractable problems involving data recovery in practical shock tests. A typical case that sometimes occurs in practice is that the accelerometer and the tested electronic devices are damaged simultaneously during the high-g shock test. As the tested device was damaged, it is compulsory to analyze the damage causes and redesign the device according to the shock environment. However, the damaged accelerometer cannot obtain the accurate shock signals to describe the shock environment. Besides, as the tested devices could be expensive, it is impermissible to perform this destructive test repeatedly. Another case is that an accelerometer without calibration is applied to shock tests due to operator's ignorance in advance. Since massive inaccurate results have been measured with the uncalibrated sensor, it is not allowable to conduct these shock tests again due to the high cost and time invested in the tests. The proposed method could pave a new avenue in addressing these kinds of data recovery problems in shock tests.

The pipeline of our work is as follows: Firstly, an experimental high-g shock environment is developed by combining a drop shock tester [1] and a dual mass shock amplifier (DMSA) [3]. This setup is pneumatic-driven with high operating efficiency, which is particularly beneficial for deep learning methods due to the low time-cost in generating and collecting abundant shock signal data. Then, a pair of faulty and working high-end accelerometers is used to measure shock signals simultaneously and continuously. After that, a pair of datasets containing shock signals from both the faulty and high-end accelerometers is collected. The failure cause of the damaged accelerometer is later diagnosed as the poor contact of the transmission line inside the faulty accelerometer. Lastly, a DNN is trained to learn the mapping between the faulty shock signals and the reference ones. A novel peak prediction network (PPN) is embedded in the DNN to ensure the accuracy of the peak value of each recovered shock signal, and this is of great benefit for the board-level drop test of electronics. The resultant network can reconstruct both the holistic time-domain shock signals and the peak values synchronously, and thus, the corrected results are suitable for both the SRS-based shock test standards and the board-level drop test standards. Experimental results show that the datasets of shock signals can be gathered with high efficiency and the trained DNN can correct the corrupted shock signals with high accuracy. This work would provide a new avenue for the research in the fields of data recovery of time-series and self-validating accelerometers.

II. The Proposed Approach

This section introduces the main components of the proposed approach. The first part demonstrates the designed high-g shock test system for generating high-g shock experiments. The second part introduces the data collection of high-g shock signals. The third part describes the structure of the DNN and how it is trained by using the collected datasets.

A. High-g Shock Test System

The first step towards building a deep learning model is to build a high-g shock test platform to generate the training data (shock signals) efficiently. There have been several types of shock test machines for generating high-g shocks [25]-[27]. Though these setups have respective advantage, such as generating higher g value, simple structure, and small size, they are too expensive and time-consuming to adapt to generate large scale data. Recently, DMSA has attracted more and more attention for high-g shock test [28]. As shown in Fig. 1, the DMSA is attached to a drop shock tester to together form a high-g shock test system. Such system can generate accelerations more than 30,000 g [29]. Its working procedures are shown in Fig. 1 (a)-(c). The DMSA is attached to a drop shock tester rigidly, which consists of a DMSA base, four guide rods, a DMSA table that moves along the guide rods freely, and bungee cords that hold the DMSA table above the base with a certain gap. To perform the high-g shock test, the drop table and DMSA will free fall together from a drop height. The drop table and DMSA base will then collide with a rubber waveform generator (RWG) fixed on the drop base in a primary impact,

and then bounce upward because of the elasticity of the RWG. Simultaneously, the DMSA table will continue moving downward and collide with the upward-moving DMSA base in a secondary impact, which generates a high-g shock signal [28].

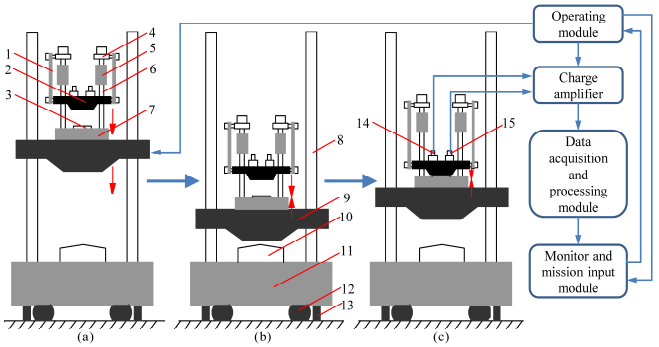

Fig. 1. The schematic of the high-g shock test system which consists of a DMSA and a drop shock tester. The DMSA is composed of 7 components, which are indexed in Fig. 1 as 1-bungee cords, 2-DMSA table, 3-DMSA programmer, 4-holders, 5-DMSA dampers, 6-DMSA guide rods, and 7-DMSA base. The drop shock tester includes 6 components, indexed in Fig. 1 as 8-drop guide rods, 9-drop table, 10-RWG, 11-drop base, 12-air springs, 13-shock tester dampers, 14-faulty accelerometer, and 15-high-end accelerometer.

Obviously, the efficiency of this shock test system primarily depends on the time-cost in lifting the drop table. We designed a pneumatic-driven shock test system as shown in Fig. 2, of which the lifting module, braking module, and air springs are all controlled by the pneumatic system. This pneumatic-driven shock test system can generate approximately 40 shock signals per minute, which is more efficient than the traditional shock testers. Additionally, the mission input module, operating module, data acquisition module, and data processing module are integrated into a control cabinet, on which all the operations for shock tests can be completed directly and all the shock signals can be collected automatically. Combining all these together, this designed high-g shock test system is greatly suitable for generating and gathering massive shock data.

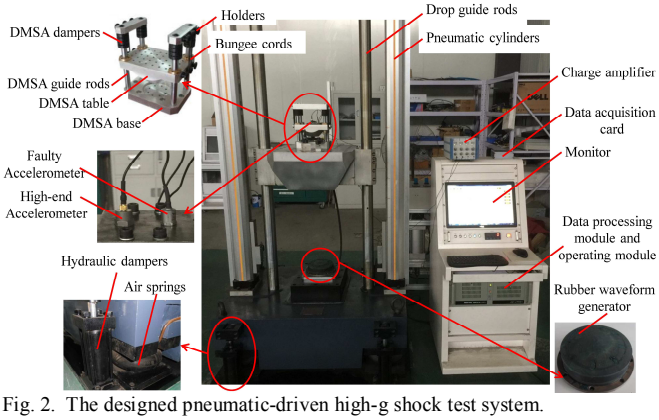

Fig. 2. The designed pneumatic-driven high-g shock test system.

B. Data Collection

As shown in Fig. 2, a faulty accelerometer (with no prior information on its fault cause but was later diagnosed as the poor contact of the transmission line inside the sensor) and an ENDEVCO® high-end accelerometer (as the ground truth) were mounted on the DMSA table closely, so that the same shock level can be measured simultaneously. The sampling rate of the data acquisition card is 200 kHz, which guarantees the sufficient fidelity for each shock signal. As an example, Fig. 3 shows a pair of signals measured from the faulty accelerometer and the high-end one respectively. Obviously, under the same shock level, the faulty accelerometer cannot measure the shock signal accurately, whereas the high-end one provides a more complete and reliable waveform.

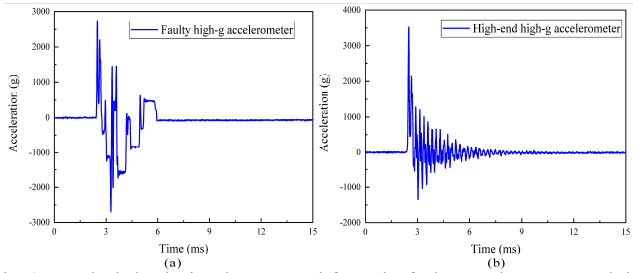

Fig. 3. Typical shock signals measured from the faulty accelerometer and the high-end accelerometer.

In order to eliminate the interference caused by the mounting positions, the mounting positions of these two accelerometers were switched and another set of shock test at the same shock level was conducted. As shown in Fig. 4, a measured shock signal after exchanging mounting position is quite in line with its initial measured shock signal, and the fitting goodness between them is 0.985, which is very close to 1. Therefore, the influences caused by the mounting positions are negligible.

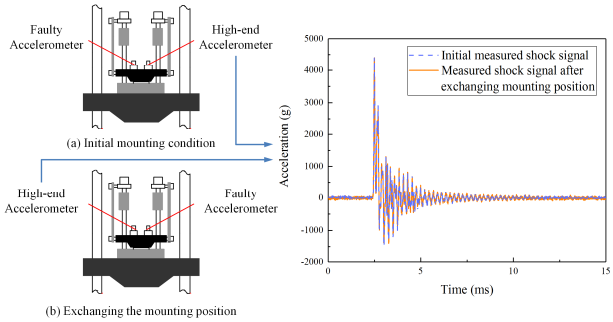

Fig. 4. The schematic of the measured shock signal after reversing mounting position and its initial measured shock signal.

After that, the drop heights were changed randomly and automatically to obtain different pairs of shock signals. These shock signals measured at different drop heights represent different shock levels. A total of 660 high-g shock tests were conducted and 660 sets of shock signal pairs were collected. Based on the peak values of all the shock signals measured by the high-end accelerometer, the distribution of the shock levels of all the data is shown in Fig. 5. Additionally, for better network training, all the measured shock signals were pre-processed to preserve the holistic temporal waveforms by removing superfluous signal: the shock signals were cut to be framed in a fixed-length temporal window of 15 ms duration, with 2.5 ms and 12.5 ms before and after their peaks respectively. Since the sampling rate is 200 kHz, each signal has a length of 3000 points. In the gathered 660 sets of shock signal pairs, 160 sets of data pairs were randomly extracted as test dataset, and the remaining 500 sets of data pairs were maintained as the training dataset for the neural network.

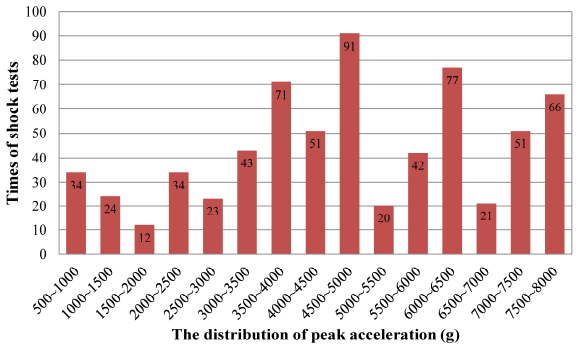

Fig. 5. The distribution of the shock levels of all the shock data.

C. The Proposed DNN

1) Overview: The inspiration of adopting deep learning to correct faulty shock signals comes from the aphorism of "diligence redeems stupidity" that humans or even biological entities can improve their skills through continuous training and effort. Moreover, recent research in applying deep learning to process time-series signals [15], [24] also proves the concept in related domains, and paves a new avenue towards the goal of this paper. Similarly, the DNN is trained with the collected shock signal datasets. Our idea is illustrated in Fig. 6, where the goal is to train a DNN that can reconstruct the corrupted signals to be as close to the reference signals as possible.

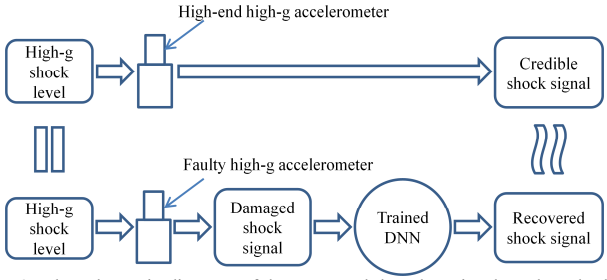

Fig. 6. The schematic diagram of the proposed deep learning-based method.

2) Autoencoder (AE): AE is a neural network designed for efficient data encoding in an unsupervised manner. The core idea of AE is to encode data in a more compact manifold than the original space through the encoder and the coding vector in the low-dimensional space can be reconstructed back to the original input space through the decoder [30]. Via enforcing the reconstruction to be as lossless as possible, AE will learn to encode the data in a most efficient way. Thusly, the coding vector is able to catch the most eminent features of the input data. Fig. 7 shows a basic AE structure with three layers.

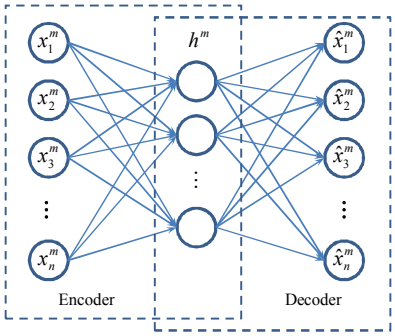

Fig. 7. The structure of an AE.

Given an unlabeled training sample set $\{\boldsymbol{x}^m\}_{m=1}^M$, the encoder transforms every training sample $\boldsymbol{x}^m$ in the set into a hidden coding vector $\boldsymbol{h}^m$ through the coding function $f_{\boldsymbol{\theta}}$, i.e.,

$$\boldsymbol{h}^m = f_{\boldsymbol{\theta}}(\boldsymbol{x}^m) = s_f(\boldsymbol{W}\boldsymbol{x}^m + \boldsymbol{b}), \quad (1)$$

where s_f is the activation function of the encoder and $\boldsymbol{\theta}=\{\boldsymbol{W},\boldsymbol{b}\}$ are the parameters of the encoder.

Then, the coding vector $\boldsymbol{h}^m$ is transformed back to a reconstruction vector $\hat{\boldsymbol{x}}^m$ by the decoding function $g_{\boldsymbol{\theta}'}$, i.e.,

$$\hat{\boldsymbol{x}}^m = g_{\boldsymbol{\theta}'}(\boldsymbol{h}^m) = s_g(\boldsymbol{W}'\boldsymbol{h}^m + \boldsymbol{d}), \quad (2)$$

where s_g denotes the activation function in the decoder, and $\boldsymbol{\theta}'=\{\boldsymbol{W}',\boldsymbol{d}\}$ are the parameters of the decoder.

The training of the entire network is done end to end by minimizing the reconstruction error $L(\hat{\boldsymbol{x}}^m,\boldsymbol{x}^m)$ of $\hat{\boldsymbol{x}}^m$ and $\boldsymbol{x}^m$. Mean square error is usually used as the standard AE loss function, such that $L(\hat{\boldsymbol{x}}^m,\boldsymbol{x}^m)$ can be expressed as:

$$L(\hat{\boldsymbol{x}}^m,\boldsymbol{x}^m) = \frac{1}{M}\sum_{m=1}^{M}\left(\frac{1}{2}\|\hat{\boldsymbol{x}}^m - \boldsymbol{x}^m\|^2\right). \quad (3)$$

If $\boldsymbol{x}^m$ can be reconstructed well from the coding vector $\boldsymbol{h}^m$, it means that most of the information contained in the training sample data are retained in the coding vector $\boldsymbol{h}^m$.

3) The Proposed DNN: Instead of the conventional approach of using AE in an unsupervised manner, it is used in a supervised fashion in this work. Furthermore, only the encoder-decoder network is not sufficient to recover the faulty shock signals because it is also supposed to have a high accuracy on the peak values of the to-be-recovered faulty shock signals. To this end, extra improvements on the structure of AE have been made. As illustrated in Fig. 8, the proposed network has three parts: encoder, decoder, and PPN, of which the PPN is introduced to handle the peak values of the shock signals specially. The input faulty signal $\boldsymbol{x}^r$ is normalized into the waveform component $\boldsymbol{x}^n$ and the peak component $\boldsymbol{p}^x$ first. The encoder and decoder network forms an AE, which has the capability to recover the entire waveform of the shock signal. The data dimension is 3000 and the feature dimension is set as 256. The PPN is an extra network branch to correct the peak value of the shock signal. It takes in both the peak value of the input shock signal $\boldsymbol{p}^x$ and the encoded global information of the normalized signal $\boldsymbol{z}$. The predicted peak value $\boldsymbol{p}^y$ and the decoded signal $\boldsymbol{y}^n$ will be un-normalized to obtain the final recovered shock signal $\boldsymbol{y}^{pred}$.

The loss function of the proposed network is as follows:

$$L = L_\infty^{shape} + L_2^{shape} + L_2^{peak}, \quad (4)$$

where $L_\infty^{shape} = \|\boldsymbol{x}^n - \boldsymbol{y}^n\|_\infty$, $L_2^{shape} = \|\boldsymbol{x}^n - \boldsymbol{y}^n\|_2$, and $L_2^{peak} = \|\boldsymbol{p}^x - \boldsymbol{p}^y\|_2$. L_∞^{shape} and L_2^{shape} are defined to encourage the transformed normalized shock signals to have similar waveforms and peak values with the reference normalized shock signals. L_2^{peak} is defined to encourage the transformed shock signals to have similar peak values with the reference counterparts. It is expected that, by minimizing these three terms, the network will be able to predict the overall waveforms of the normalized shock signals as well as the peak values accurately. Adam optimizer [31] with a learning rate of 1×10^{-4} is used. The convergence of the network training process is shown in Fig. 9. It can be seen that, although the losses are of different magnitudes, both of them converges well thanks to the network designing and training protocol.

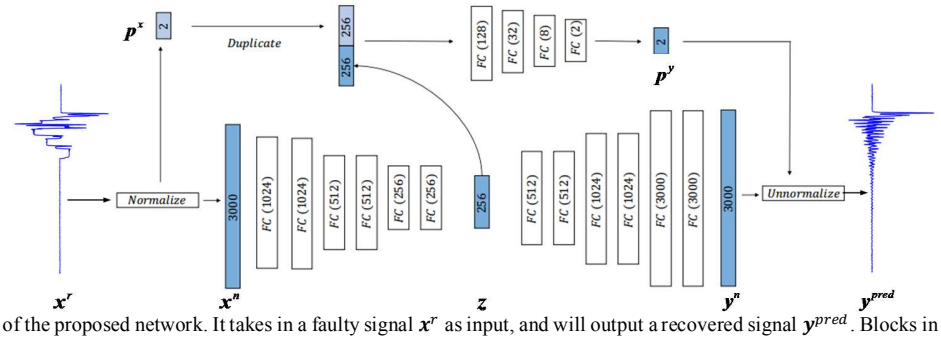

Fig. 8. The architecture of the proposed network. It takes in a faulty signal $\boldsymbol{x}^r$ as input, and will output a recovered signal $\boldsymbol{y}^{pred}$. Blocks in color denote tensors, and transparent blocks denote network layers. Numbers in the block corresponds to the feature dimensions.

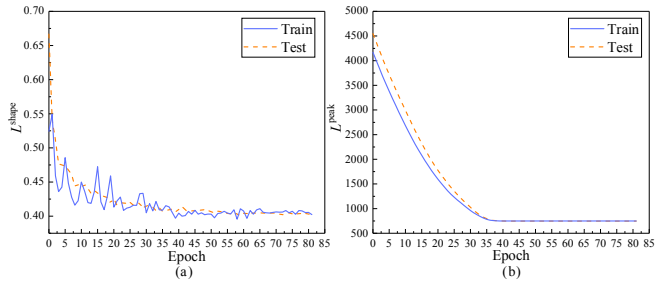

Fig. 9. The convergence curves of the proposed network. Shown in the figure are (a) the convergence curve of the loss of the overall shock waveforms and (b) the convergence curve of the loss of the peak values.

III. Experimental Results

A. Error Metrics

To thoroughly investigate the performance of our approach, several metrics are proposed to quantify the signal recovery quality: 1) relative error of peak values (REP), 2) SRS curves, 3) difference of time-domain waveforms (DTW), and 4) determination coefficient (R^2), by comparing the recovered shock signal with the corresponding reference signal.

The metric of REP is defined as:

$$\mathrm{REP} = |y_{\max}^{Rec} - y_{\max}^{Ref}|/y_{\max}^{Ref}, \tag{5}$$

where $y_{\max}^{Rec}$ and $y_{\max}^{Ref}$ is the maximal g value of the recovered shock signal series ($\boldsymbol{y}^{Rec}$) and the reference shock signal series ($\boldsymbol{y}^{Ref}$) respectively. This evaluation index describes the ability of recovering maximal shock responses from the faulty signals. Considering that the peak value is a key index in board-level shock test standards [3], [28], [29], it is essential to require the proposed approach to recover the peak values from the faulty shock signals, and so that the recovered results could be used to assess the reliability of products during board-level shock tests.

Another error metric is the SRS curve which is a presentation for shock signals in frequency domain and serves as an important characteristic in the pyroshock test standards [2], [6]. The SRS curve is obtained by imposing the shock signal into a series of single degree of freedom mass-spring systems with increasing natural frequencies, and computing the maximal absolute acceleration response against its corresponding natural frequency [2]. It can be plotted with the improved recursive filter method quickly, but the whole time-domain signal must be provided in advance. Thus, it is essential for the proposed method to be able to recover the holistic time-domain shock signal as complete as possible, such that the recovered shock signals could be converted to the SRS curves and used to assess the reliability of products during the pyroshock tests directly.

The third metric of DTW can be obtained by:

$$\mathrm{DTW} = (y_i^{Rec} - y_i^{Ref})/\, y_{\max}^{Ref}, i = 1, 2, \cdots, n, \tag{6}$$

in which y_i^{Rec} and $y_{\max}^{Ref}$ is the value of the i-th point in $\boldsymbol{y}^{Ref}$ and the maximal value of $\boldsymbol{y}^{Ref}$ respectively. This assessing index describes the local accuracy of every point in the recovered shock signal. The smaller the DTW is, the higher the local accuracy of the point.

Lastly, we also compute the determination coefficient of the recovered shock signal, which is defined as:

$$R^2 = 1 - \sum_1^n \left(y_i^{Rec} - y_i^{Ref}\right)^2 / \sum_1^n (y_i^{Rec} - \bar{y}^{Ref})^2, \tag{7}$$

where $\bar{y}^{Ref}$ is the mean of $\boldsymbol{y}^{Ref}$. This metric indicates the global accuracy of the recovered shock signal. R^2 will be close to 1 with a high global accuracy of the recovered results.

B. Visualization of the network calibration

As shown in Fig. 10, the faulty high-g accelerometer produces corrupted high-g shock signals. By comparing the recovered signals and the reference signals, it can be found that the shock signals recovered by the DNN match closely, in terms of their overall temporal waveforms, with the corresponding reference signals. This is highly desirable and indicates that the holistic time-domain faulty shock signals can be confidently and effectively recovered by the proposed method. On the other hand, the SRS curves of the recovered shock signals and the corresponding reference signals also match very well. The SRS curves of the faulty shock signals are clearly deviating from the reference data. This not only implies the validity of the proposed method, but also verifies that the recovered signals can be applied into the pyroshock test directly and accurately.

In terms of the errors in the time domain, the local relative errors of the sampling points in the recovered signals mostly fall below 15%, with few outliers ranging from 15% to 20%. It is considered that the local accuracy of the recovered signals is averagely satisfactory. Considering the high data-loss of the faulty sensor, ensuring the accuracy of all individual sampling points is very difficult and is not the main focus of this work. Reducing the local errors of the recovered shock signals will be the next research direction to improve our proposed algorithm.

C. Qualitative Comparison

The peak values, REPs, maximal DTWs and R^2 values of the results in Fig. 10 are summarized in Table I. It can be seen that the REPs are all below 15%. This is of vital importance for the shock test of electronics because the permissible error is less than 20% in several shock test standards, such as JESD22-BI11 [32] and IEC 60068-2-27: 2008 [33]. Additionally, the R^2

values are all more than 0.921, which is very close to 1, showing a highly fitting accuracy between the recovered signals and the reference signals. Also, these R^2 values imply the high global accuracy of the shock signals recovered by the proposed method. Besides, most of the maximal DTWs are below 15%, which indicates that the local accuracy of the recovered signals is generally adequate. However, it still needs to be improved to further reduce the DTW indices in future.

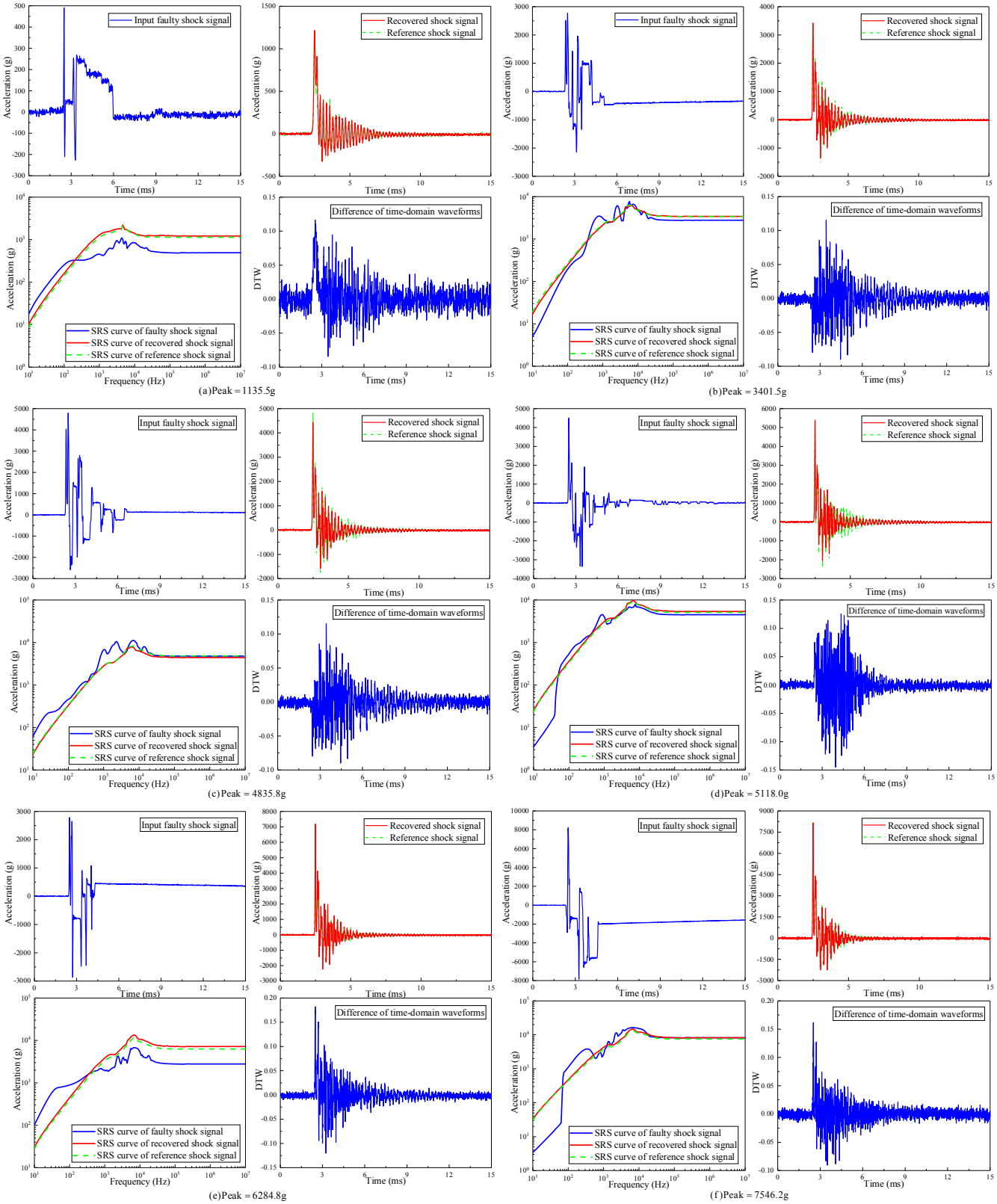

Fig. 10. Visualization of the shock signals before and after correction. Better to be viewed in color.

TABLE I
THE PEAK VALUES, REPS, MAXIMAL DTWS AND R^2 VALUES OF THE RESULTS ILLUSTRATED IN FIG. 10.

Sequence of the results	Recovered peak value (g)	Reference peak value (g)	REP (%)	R^2	Maximal DTW (%)
Fig. 10(a)	1216.0	1135.5	7.09	0.968	11.64
Fig. 10(b)	3423.6	3401.5	0.65	0.959	11.52
Fig. 10(c)	4429.6	4835.8	8.40	0.946	12.19
Fig. 10(d)	5384.9	5118.0	5.22	0.921	12.55
Fig. 10(e)	7182.9	6284.8	14.29	0.949	18.21
Fig. 10(f)	8168.0	7546.2	8.24	0.961	16.18

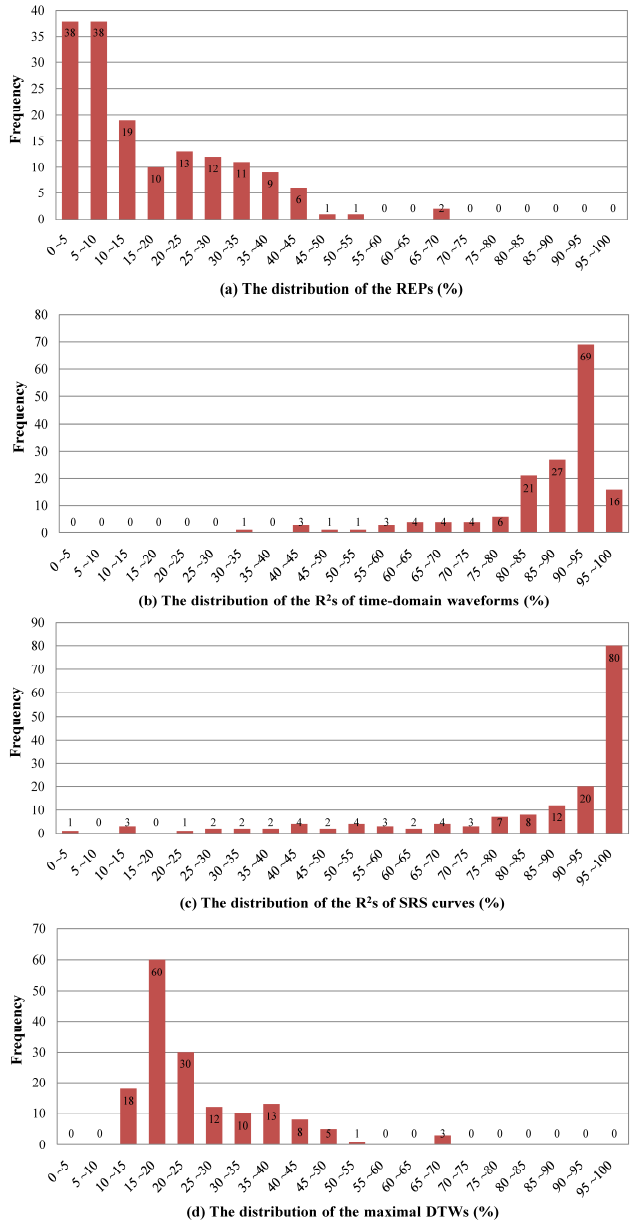

Fig. 11. The distributions of the error metrics of the recovered signals.

To further illustrate the effectiveness of our proposed network, the distributions of the recovery results of the test dataset are demonstrated in Fig. 11. It can be seen that most REPs between the recovered signals and the reference signals are distributed in 0-25%, which illustrates that the designed network has desirable performance in predicting the peaks. This performance could be attributed to the customized PPN.

It can be seen from Fig. 11 (b) that most of the R^2 values between the recovered time-domain shock signals and their counterparts are higher than 80%, which is very close to 1. This implies that our proposed network is considerably capable of predicting the overall waveforms of the shock signals. Similarly, as demonstrated in Fig. 11 (c), most of the R^2 values of the SRS curves between the recovered shock signals and the reference signals are above 80% that also confirms the validity of applying our proposed method for the pyroshock tests.

Fig. 11 (d) demonstrates that most of the maximal DTWs between the recovered shock signals and their counterparts are distributed from 10% to 25%, which shows that the designed network has a moderate performance in keeping the local accuracy of the recovered signals. There are still few outliers in Fig. 11 distributed in the unsatisfactory ranges, and it would be our further investigation to improve the network performance.

IV. CONCLUSION

In this paper, we proposed a deep learning-based approach to recover faulty high-g shock signals. To obtain the training data, a high-g shock test system is firstly developed by combining a pneumatic-driven drop shock tester and a DMSA. We proposed a network that comprises encoder, decoder, and PPN that enhances the prediction of the peak values. Trained with the extensive data collected, this network has shown highly promising performance in mapping the faulty signals into their correct counterparts accurately and effectively.

Unlike repairing hardware, the proposed method is purely data-driven and has advantages of low cost, high efficiency, and great generalization performance. Besides, this approach can reconstruct the whole time-domain signals and peak values synchronously, hence suitable for both the pyroshock test and board-level shock test simultaneously. Lastly, the performance is not affected by the low repeatability of the corrupted signals.

Our proposed method is currently developed under a standard shock test environment and benchmarked on a typical fault type. However, we believe the methodology can be suitable for more cases that would require more testing for further verification, investigation, and improvement. On the other hand, this method may not be able to adapt to all kinds of shock environments. Likewise, it does not mean that all kinds of faulty signals can be recovered by this method. We will next focus on better understanding the boundary of the DNN-based data reconstruction in terms of fault types or data corruption level and also improving our strategy to be suitable for more acceleration measuring conditions.

REFERENCES

[1] J. Wen, C. Liu, H. Yao, and B. Wu, "A nonlinear dynamic model and parameters identification method for predicting the shock pulse of rubber waveform generator," *Int. J. Impact. Eng.*, vol. 120, pp. 1-15, Oct. 2018.
[2] O. M. F. Morais and C. M. A. Vasques, "Shock environment design for space equipment testing," *P. I. Mech. Eng. G-J. Aer*, vol. 231, no. 6, pp. 1154-1167, 2017.
[3] J. Meng, S. T. Douglas, and A. Dasgupta, "MEMS packaging reliability in board-level drop tests under severe shock and impact loading conditions–Part I: experiment," *IEEE Trans. Comp. Pack. Man.*, vol.6, no.11, pp.1595-1603, 2016.
[4] G. Sun, F. Xu, G. Li, and Q. Li, "Crashing analysis and multiobjective optimization for thin-walled structures with functionally graded thickness,"

Int. J. Impact. Eng., vol. 64, pp. 62-74, Feb. 2014.
[5] V. Narasimhan, H. Li, and M. Jianmin, "Micromachined high-g accelerometers: a review," *J. Micromech. Microeng.*, vol. 25, no. 3, pp. 033001, 2015.
[6] A. García-Pérez, F. Sorribes-Palmer, G. Alonso, and A. Ravanbakhsh, "Overview and application of FEM methods for shock analysis in space instruments," *Aerosp. Sci. Technol.*, vol. 80, pp. 572-586, Jul., 2018.
[7] Y. Zhao, X. Li, J. Liang, and Z. Jiang, "Design, fabrication and experiment of a MEMS piezoresistive high-g accelerometer," *J. Mech. Sci. Technol.*, vol. 27, no. 3, pp. 831-836, 2013.
[8] Methods for the calibration of vibration and shock transducers—Part 13: primary shock calibration using laser interferometry, ISO 16063-13, 2001.
[9] Methods for the calibration of vibration and shock transducers—Part 22: shock calibration by comparison to a reference transducer, ISO 16063-22, 2005.
[10] Z. Pang, Y. Liu, M. Li, C. Zhu, S. Li, Y. Wang, ..., and C. Song, "Influence of process parameter and strain rate on the dynamic compressive properties of selective laser-melted Ti-6Al-4V alloy," *Appl. Phys. A-Mater.*, vol. 125, no. 2, pp. 90, 2019.
[11] S. H. Choy, X. X. Wang, H. L. W. Chan, and C. L. Choy, "Electromechanical and ferroelectric properties of (Bi1/2Na1/2) TiO3-(Bi1/2K1/2) TiO3-(Bi1/2Li1/2) TiO3-BaTiO3 lead-free piezoelectric ceramics for accelerometer application," *Appl. Phys. A-Mater.*, vol. 89, no. 3, pp. 775-781, 2007.
[12] Z. Feng, Q. Wang and S. Katsunori, "Sensor fault detection and data recovery based on LS-SVM predictor," Chinese J. Sci. Instrum., vol. 28, no. 2, pp. 193-197, 2007.
[13] Y. Wang, J. Fan, J. Zu, and P. Xu, "Quasi-static calibration method of a high-g accelerometer," *Sensor.*, vol. 17, no. 2, pp. 409, 2017.
[14] A. Link, A. Täubner, W. Wabinski, T. Bruns, and C. Elster, "Calibration of accelerometers: determination of amplitude and phase response upon shock excitation," *Meas. Sci. Technol.*, vol. 17, no. 7, pp. 1888, 2006.
[15] H. Song, J. J. Thiagarajan, P. Sattigeri, and A. Spanias, "Optimizing kernel machines using deep learning," *IEEE Trans. Neur. Net. Lear.*, vol. 29, no. 11, pp. 5528-5540, 2018.
[16] G. Jiang, H. He, J. Yan, and P. Xie, "Multiscale convolutional neural networks for fault diagnosis of wind turbine gearbox," *IEEE Trans. Ind. Electron.*, vol. 66, no. 4, pp. 3196-3207, Apr. 2019.
[17] Y. Yu, H. Yao, and Y. Liu, "Aircraft dynamics simulation using a novel physics-based learning method," *Aerosp. Sci. Technol.*, vol. 87, pp. 254-264, Apr., 2019.
[18] H. S. Oh, U. Kim, G. Kang, J. K. Seo, and H. R. Choi, "Multi-axial force/torque sensor calibration method based on deep-learning," *IEEE Sens. J.*, vol. 18, no. 13, pp. 5485-5496, 2018.
[19] Z. Feng, Q. Wang, and S. Katsunori, "Design and implementation of a self-validating pressure sensor," *IEEE Sens. J.*, vol. 9, no. 3, pp. 207-218, 2009.
[20] J. Yu, J. Li, Q. Dai, D. Li, X. Ma, and Y. Lv, "Temperature compensation and data fusion based on a multifunctional gas detector," *IEEE Trans. Instrum. Meas.*, vol. 64, no. 1, pp. 204-211, 2015.
[21] B. Liu, T. Han, and C. Zhang, "Error correction method for passive and wireless resonant saw temperature sensor," *IEEE Sens. J.*, vol. 9, no. 3, pp. 3608-3614, 2015.
[22] Y. Chen, S. Jiang, J. Yang, K. Song, and Q. Wang, "Grey bootstrap method for data validation and dynamic uncertainty estimation of selfvalidating multifunctional sensors," *Chemometrics Intell. Lab. Syst.*, vol. 146, pp. 63-76, Aug. 2015.
[23] S. Ryan, S. Thaler, S. Kandanaarachchi, "Machine learning methods for predicting the outcome of hypervelocity impact events," *Expert Syst. Appl.*, vol. 45, no. 1, pp. 23-39, Mar. 2016.
[24] H. Yao, J. Wen, Y. Ren, B. Wu, and Z. Ji, "Low-cost measurement of industrial shock signals via deep learning calibration," in *Proc. ICASSP*, Brighton, UK, 2019, pp. 2892-2896.
[25] G. Kelly, J. Punch, S. Goyal, and M. Sheehy, "Shock pulse shaping in a small-form factor velocity amplifier," *Shock Vib.*, vol. 17, no. 6, pp. 787-802, 2010.
[26] K. Dai, X. Wang, F. Yi, Y. Yin, C. Jiang, ..., and Z. You, "Discharge voltage behavior of electric double-layer capacitors during high-g impact and their application to autonomously sensing high-g accelerometers," *Nano Res.*, vol. 11, no. 2, pp. 1146-1156, 2018.
[27] X. Zhang, Y. Zhao, Z. Duan, and X. Li, "A high-g shock tester with one-level velocity amplifier," *Meas. Sci. Technol.*, vol. 24, no. 4, pp. 045901, 2013.
[28] A. Zhang, "High acceleration board level reliability drop test using dual mass shock amplifier," in *Proc. ECTC*, Orlando, FL, USA, 2014, pp. 1441-1448.
[29] S. T. Douglas, M. Al-Bassyiouni, A. Dasgupta, K. Gilman, and A. Brown, "Simulation of secondary contact to generate very high accelerations," *J. Electron. Packaging*, vol. 137, no. 3, pp. 031011, 2015.
[30] J. Zabalza, J. Ren, J. Zheng, H. Zhao, C. Qing, Z. Yang, ..., and S. Marshall, "Novel segmented stacked autoencoder for effective dimensionality reduction and feature extraction in hyperspectral imaging," *Neurocomputing*, vol. 185, pp. 1-10, 2016.
[31] D. P. Kingma and J. Ba, "Adam: A method for stochastic optimization," in *Proc. ICLR*, San Diego, CA, USA, 2015, pp. 1-15.
[32] Board level drop test method of components for handheld electronic products, JESD22-BI11, 2003.
[33] Environment testing-Part 2-27: Tests-Test Ea and guidance: Shock, IEC 60068-2-27, 2008.

Jingjing Wen received his B.S. degree and M.Sc. degree from School of Astronautics, Northwestern Polytechnical University, Xi'an, China, in 2013 and 2016 respectively. Currently, he is a Ph.D. candidate in Northwestern Polytechnical University. From Jul. 2019 to the current, he worked in Cardiff University, UK as a Research Associate. So far, he has more than 12 papers published. His main research interests include shock test, intelligent testing instrumentation, and self-validating sensor.

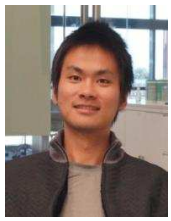

H**oupu Yao** (GS'15) obtained his Ph.D. degree in Aerospace Engineering from Arizona State University, Tempe, Arizona, USA. He received his bachelor degree from Northwestern Polytechnical University, Xi'an, Shaanxi, in 2013. His research interests include computational mechanics and acoustics, deep learning and computer vision, parallel computation, and material design. His current interest is in autonomous driving.

Bin Wu received his B.S. degree and M.Sc. degree from School of Astronautics, Northwestern Polytechnical University, Xi'an, China, in 1987 and 1998 respectively. Currently, he is an associated professor in Northwestern Polytechnical University. So far, he has more than 50 papers published and held more than 10 national patents. His main research interests include mass property measurement technique, test technology of mechanical environment, and sensor fault diagnosis.

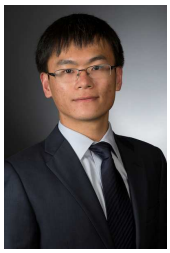

Yi Ren is an Assistant Professor in Mechanical Engineering at Arizona State University. He received his Ph.D. in Mechanical Engineering from the University of Michigan in 2012 and his B.Eng. degree in Automotive Engineering from Tsinghua University in 2007. From 2012 to 2014 he was a postdoctoral researcher at the University of Michigan, leading projects on automated hybrid powertrain design, large-scale consumer preference learning, and government policy design for electric vehicle markets. Dr. Ren's current research focuses on the development of robust machine learning mechanisms for risk-sensitive tasks, with particular focus on accelerated computational engineering design and verifiable human-machine interactions. His work on optimal design through crowdsourcing received the Best Paper Award in Design Automation at the 2015 ASME International Design and Engineering Technical Conferences.

Ze Ji (M'19) is a lecturer at the school of Engineering, Cardiff University, UK. He received his BEng (2001) from Jilin University, China, MSc (2003) from the University of Birmingham, UK, and PhD (2007) from Cardiff University, UK. Prior to his current position, he was working in industry on autonomous robotics. His research interests are cross-disciplinary, with a focus on autonomous robot navigation, computer vision, simultaneous localization and mapping (SLAM), machine learning, unmanned surface vehicles, and acoustic localization.